Bioinformatics-based Identification of the Mechanism Whereby Astragalus Membranaceus Inhibits Inflammation and Autophagy in Lupus Nephritis

Ting Liu
the First Hospital of Shanxi Medicial University
Xiaomei Qiao
Shanxi Medicial University
Kaili Kong
Shanxi Medicial University
XiaoXia Wang
Shanxi Medicial University
Rui Li
Shanxi Medicial University
Xiaodong Zhang (zxdspl@163.com)
the First Hospital of Shanxi Medicial University

Research Article

Keywords: Astragalus membranaceus, inflammation, autophagy, lupus nephritis, Weight Gene Co-expression Network Analysis

Posted Date: October 13th, 2021

DOI: https://doi.org/10.21203/rs.3.rs-936493/v1

Abstract

Background. Lupus nephritis (LN) is an autoimmune disease, and effective treatment can improve the prognosis of patients. Several studies have demonstrated that Astragalus membranaceus can effectively suppress the progression of LN, but the underlying mechanism is still unclear. Thus, this study aimed to investigate the mechanism whereby Astragalus membranaceus exerts this therapeutic effect against LN.

Method. Astragalus targets and LN-related targets were obtained from the TCMSP database and WGCNA analysis, respectively. Then we obtain the compound targets and constructed the protein interaction network of the compound targets. The top 10 core targets were identified. And We have validated it. We performed GO and KEGG enrichment analyses on the compound targets to identify the functional and genomic pathways enriched among these targets. Molecular docking of Astragalus membranaceus with the core targets was performed .

Result. We identified 214 AM targets and 102 LN-related targets. Among them, we obtained 10 core targets, IL-1β, EGF, CCND1, CASP3, STAT1, PTGS2, and PPARγ were found to have high diagnostic values for LN. In the validation dataset GSE99339, all the core targets were significantly expressed, except for EGF deletion. The results of the KEGG enrichment analysis showed that 7 out of 23 valid targets were significantly enriched in the mitogen-activated protein kinase pathway (p=1.14E-05). The molecular-docking results showed that AM with IL-1β, CASP3, STAT1, and PPARγ had good binding properties.

Conclusion. The therapeutic effect of AM against LN might be related to suppression of inflammation and autophagy, and the bioinformatics-based results presented here provide a theoretical basis for the clinical application of AM in LN.

Highlights

1. The combination of bioinformatics analysis and network pharmacology were applied.
2. 4 key genes are associated with the mechanism whereby Astragalus membranaceus for lupus nephritis.
3. We predicted that AM for LN might be related to inflammation and autophagy.

1. Introduction

Systemic lupus erythematosus (SLE) is an autoimmune disease with multi-organ involvement [1]. Lupus nephritis (LN) is one of the most severe complications of SLE. Approximately 5–20% of LN cases progress to end-stage renal disease (ESRD), a significant cause of death in SLE [2, 3]. The treatment of LN mainly relies on hormones and immunosuppressants. However, the majority of patients are still not effectively controlled and progress to ESRD. Therefore, it is crucial to identify effective targets to suppress the progression of LN.

Astragalus membranaceus (AM) is a legume that has a variety of bioactive components such as astragaloside, astragalus polysaccharide and astragalus flavonoids [4, 5]. And it is one of the most widely used herbal remedies for kidney diseases. Studies have proved that it has the effect of reducing proteinuria, reducing creatinine, anti-inflammation and regulating immunity. AM significantly reduces the expression of inflammatory genes and cytokines in LN and suppresses the progression of this disease[6, 7]. However, the factors involved and their specific mechanisms remain unclear.

Weighted gene co-expression network analysis (WGCNA) is a systematic biological analysis that identifies the core genes associated with a disease. Network pharmacology has unique advantages in analyzing herbal medicines with multiple components and targets. Therefore, this study aimed to investigate the core genes and possible mechanisms whereby AM suppresses LN. The flow diagram of this study was showed in Fig. 1.We present the protocol in accordance with the STARD reporting checklist

2. Materials And Methods

2.1 Acquisition of the therapeutic targets of AM

The bioactive ingredients of AM and their corresponding target genes were retrieved from the Traditional Chinese Medicine Systematic Pharmacology Database and Analysis Platform (TCMSP, http://lsp.nwu.edu.cn/tcmsp.php). The screening criteria for the bioactive ingredients were to meet both oral bioavailability (OB) ≥ 30% and drug-likeness (DL) ≥ 0.18. We removed duplicate, non-human, meaningless targets, and the remaining targets were entered into the Uniprot database and converted into genes to obtain the therapeutic targets of AM.

2.2 Lupus nephritis microarray data collection and pre-processing

We searched for “lupus nephritis” in the National Center for Biotechnology Information Gene Expression Database (GEO, http: //www.ncbi.nlm.nih.gov/GEO/) and downloaded the data that are from gene microarrays and gene array platforms and that met the criteria. Then the microarray data were annotated for the next step of WGCNA. The screening criteria were as follows: 1) the study species was human, and the microarray data were derived from the kidney, not blood or urine; 2) the sample size was > 20; and 3) both LN group and healthy control group were included, and the complete gene microarray data and platform data were available.

2.3 Construction of the weighted gene co-expression network

Significant outlier samples were first identified and removed by calculating the inter-array correlation of the dataset. We calculated the Pearson correlation coefficient between gene expressions for the remaining samples by applying the power adjacency function in the "WGCNA" package of R (3.6.3)

software. Afterward, we filtered the best soft threshold (β) by the "pick Soft Threshold" function to construct a scale-free gene co-expression network.

The "dissimilarity" function in the "WGCNA" package was used to first cluster the genes in the microarray dataset and construct a hierarchical clustering tree to cluster the genes with similar functions into the same gene module. Then, we set the minimum number of genes in each module to 50 and the cut height to 0.25 and used the Dynamic tree cut method to divide the gene modules. We calculated the module eigengene (ME), modular membership (MM), and gene significance (GS), and the modular genes with high GS and high MM were selected as the LN-related targets.

2.4 Construction of protein-protein interaction (PPI) and "drug-bioactive ingredients-compound targets-disease" interaction networks

We applied the "Venn Diagram" package in R3.6.3 software to match the targets of AM with the targets related to LN to obtain the AM-LN compound targets. The compound targets were imported into the STRING database (https://www.string-db.org), and the species was restricted to "Homo sapiens" to obtain the PPI network. The PPI network was visualized and analyzed using the Cytoscape 3.8.2 software. The top 10 target genes were selected as the core targets by using degree value. The compound targets and their corresponding bioactive ingredients were also imported into Cytoscape 3.8.2 to generate a "drug-bioactive ingredients-compound targets-disease" network.

2.5 Gene Ontology (GO) and Kyoto Encyclopedia of Genes and Genomes (KEGG) enrichment analyses

We used the "Cluster Profiler GO" and "Cluster Profiler KEGG" packages in R to perform GO and KEGG enrichment analyses on the compound targets. Then, we generated histograms and bubble plots. Satisfying "q value < 0.01 and corrected p-value < 0.01" was considered biologically significant.

2.6 Clinical internal validation of the core genes

GSE32591 clinical data from the European Renal Disease Database (https://www.nephroseq.org/resource/login.html) were downloaded. After screening for the variables via logistic regression analysis, a columnar plot of the risk of developing LN was constructed and validated. Then, we calculated the area under the ROC curve (AUC) for 10 core genes by using the "pROC" package of R to assess the diagnostic value of each gene. We identified the genes with AUC > 0.7 as clinically significant for LN.

2.7 External verification

The GEO database (http://www.ncbi.nlm.nih.gov/geo) was searched again for "lupus nephritis" to identify another LN dataset—GSE99339. We again compared the expression levels of the 10 core genes between the LN group and the healthy control group in GSE99339 microarray data to further validate the clinical significance of the 10 core genes for LN.

2.8 Molecular docking

We identified four key genes after combining the degree and AUC values, and we downloaded the crystal structures of the proteins encoded by these key targets and the 3D structures of the bioactive ingredients corresponding to the most bioactive targets from the Protein Data Bank (PDB, http://www.pdb.org/) and PubChem database, respectively. We processed the 3D structures and bioactive ingredients by using the PyMol software. Then, we performed molecular docking by using the AutoDock Tools 1.5.6 software after adding hydrogen atoms and calculating the charges. A Lamarckian genetic algorithm was used to record the lowest binding energy and the best corresponding conformation[8–10]. Binding energy < 0 indicated that the ligand can bind to its receptor spontaneously, and a binding energy ≤ -5.0 $kJ \cdot mol^{-1}$ was considered to be an excellent binding property.

3. Results

3.1 Acquisition of AM targets

We identified 87 bioactive ingredients of AM from the TCMSP database. Among them, 17 satisfied the conditions of OB ≥ 30% and DL ≥ 0.18 (Table 1). The obtained action targets were entered into the Uniprot database (https://www.uniprot.org/) to eliminate any meaningless target. Finally, we obtained 302 target genes as the action targets of AM.

Table 1
Bioactive ingredients of AM and their characteristics

MolID	MoleculeName	OB(%)	DL
MOL000211	Mairin	55.38	0.78
MOL000239	Jaranol	50.83	0.29
MOL000296	hederagenin	36.91	0.75
MOL000033	(3S,8S,9S,10R,13R,14S,17R)-10,13-dimethyl-17-((2R,5S)-5-propan-2-yloctan-2-yl)-2,3,4,7,8,9,11,12,14,15,16,17-dodecahydro-1H-cyclopenta(a)phenanthren-3-ol	36.23	0.78
MOL000354	isorhamnetin	49.60	0.31
MOL000371	3,9-di-O-methylnissolin	53.74	0.48
MOL000378	7-O-methylisomucronulatol	74.69	0.30
MOL000379	9,10-dimethoxypterocarpan-3-O-β-D-glucoside	36.74	0.92
MOL000380	(6aR,11aR)-9,10-dimethoxy-6a,11a-dihydro-6H-benzofurano(3,2-c)chromen-3-ol	64.26	0.42
MOL000387	Bifendate	31.10	0.67
MOL000417	Calycosin	47.75	0.24
MOL000422	kaempferol	41.88	0.24
MOL000433	FA	68.96	0.71
MOL000439	isomucronulatol-7,2'-di-O-glucosiole	49.28	0.62
MOL000442	1,7-Dihydroxy-3,9-dimethoxypterocarpene	39.05	0.48
MOL000098	quercetin	46.43	0.28

3.2 Acquisition and pre-processing of LN-related gene-microarray data

We obtained dataset GSE32591 and platform data GPL14663 from the GEO database. This database contains 14 cases of healthy individuals and 32 cases of LN patients. We converted the gene IDs in the GSE32591 dataset to the gene names (gene symbols) in the GPL14663 platform dataset and removed the vacant values and duplicate genes, and we finally obtained 12548 genes for subsequent analyses.

3.3 Weighted gene co-expression network analysis

We performed WGCNA on 46 samples and 12548 genes. After normalization, we detected no significant outlier samples. A scale-free network was constructed by choosing $\beta = 5$ (scale-free $R^2 = 0.99$) (Fig. 2). The minimum number of genes per module was set to 50, and the shearing height was 0.25 for dynamic

shearing. Consequently, 12 gene modules were obtained (Fig. 3). The number of genes contained in each module is shown in Table 2.

Table 2
Number of genes in each module

Module	Number of genes
Tan	73
Yellow	339
Salmon	53
Magenta	105
Brown	476
Purple	89
Pink	117
Turquoise	1347
Black	147
Blue	1029
Red	305
Grey	1

By calculating ME, MM, and GS, the modules were correlated with clinical features. We considered the blue module (R = 0.84 and P = 3e-13) as the central module (Fig. 4), and the module gene as the most closely related to LN. **fig.s 5A and 5B** show the connectivity alongside the importance of the genes within the blue modules in the LN and healthy groups, respectively, with $p < 0.05$.

3.4 PPI network and "drug-bioactive ingredients-compound targets-disease" interaction network

We screened 24 AM and LN compound targets by using the R software VennDiagram data package (Fig. 6) and imported 24 compound targets into the STRING database for protein-interaction analysis, PPI network diagram (Fig. 7A), and string interactions. We imported the tsv files into the Cytoscape 3.8.2 software, and the top 10 targets, namely *IL-1β*, *EGF*, *CASP3*, *CCND1*, *STAT1*, *PTGS2*, *PPARγ*, *AR*, *CXCL10*, and *KDR* (ordered according to degree value), were identified as the core targets of AM in the treatment of LN (Table 3 **and** Fig. 7B).

Table 3
Core targets of AM in the treatment of LN

rank	name	score	rank	name	score
1	*IL1β*	23	6	*PTGS2*	21
2	*EGF*	23	7	*PPARγ*	20
3	*CASP3*	22	8	*AR*	18
4	*CCND1*	22	9	*CXCL10*	17
5	*STAT1*	21	10	*KDR*	16

We used Cytoscape 3.8.2 to construct the "drug-bioactive ingredients-compound targets-disease" network diagram. The nodes correspond to the drug name, the bioactive ingredient, core target, and disease (Fig. 8). The full names of the bioactive ingredients and their corresponding abbreviations are shown in Table 4. HQ17 (quercetin) connects with the most targets (n = 153), followed by HQ13 (kaempferol) (n = 85). Therefore, quercetin and kaempferol are the first and second main bioactive components of AM, respectively.

Table 4
Full names and abbreviations of the bioactive ingredients

full name	abbreviations
Mairin	HQ1
Jaranol	HQ2
hederagenin	HQ3
(3S,8S,9S,10R,13R,14S,17R)-10,13-dimethyl-17-((2R,5S)-5-propan-2-yloctan-2-yl)-2,3,4,7,8,9,11,12,14,15,16,17-dodecahydro-1H-cyclopenta(a)phenanthren-3-ol	HQ4
isorhamnetin	HQ5
3,9-di-O-methylnissolin	HQ6
7-O-methylisomucronulatol	HQ7
9,10-dimethoxypterocarpan-3-O-β-D-glucoside	HQ8
(6aR,11aR)-9,10-dimethoxy-6a,11a-dihydro-6H-benzofurano(3,2-c)chromen-3-ol	HQ9
Bifendate	HQ10
formononetin	HQ11
Calycosin	HQ12
kaempferol	HQ13
FA	HQ14
isomucronulatol-7,2'-di-O-glucosiole	HQ15
1,7-Dihydroxy-3,9-dimethoxypterocarpene	HQ16
quercetin	HQ17

3.5 GO and KEGG enrichment analyses

GO and KEGG enrichment analyses were performed on 24 compound targets by using the "Bioconductor" function in R. The GO enrichment results showed that 24 compound targets were involved in cell growth and regulation and were related to biological processes such as endothelial cell proliferation (Fig. 9A, B). To gain further insight into the pharmacological mechanisms of AM in LN, we performed the KEGG pathway analysis. Finally, 88 biologically significant pathways were obtained (q-value < 0.01 and corrected p-value < 0.01), among which 7 of the 23 genes (*CASP3*, *EGF*, *KDR*, *IL-1β*, *IKBKB*, *INSR*, and *PRKCB*) were enriched in the mitogen-activated protein kinase (MAPK) signaling pathway with p-value = 1.14E-05, suggesting that AM may interfere with this signaling pathway in the treatment of LN (Fig. 9C, D).

3.6 Clinical internal validation of the core genes

The nomogram (Fig. 10A) showed good distinction and calibration in predicting the risk of LN, with the AUC value of 0.886 (Fig. 10B). The calibration curve showed good agreement between the LN risk predicted by the nomogram and the actual risk of LN (Fig. 10C).

The AUC values of the top 10 core genes identified from the GSE32591 dataset were calculated using the "pROC" function in the R package to investigate the diagnostic performance of the core genes for LN. The results showed that *IL1B*, *EGF*, *CCDN1*, *CASP3*, *STAT1*, *PTGS2*, *AR*, and *PPARγ* had diagnostic values for LN. Among the screened core genes, *CCDN1*, *STAT1*, and *PPARγ* had the highest diagnostic values (Fig. 11).

3.7 External validation

Another LN dataset, GSE99339, was identified from the GEO database to compare the expression levels of the core genes between the LN and healthy groups. The results showed that the core genes, except for *EGF*, (*IL1*, *CCND1*, *CASP3*, *STAT1*, *PTGS2*, *PPARγ*, *AR*, *CXCL10*, and *KDR*) were significantly upregulated in GSE99339 (Fig. 12).

3.8 Molecular docking

We used the Autodock software to molecularly dock four key targets (*STAT1*, *PPARγ*, *IL-1β*, and *CASP3*) with quercetin, the first major bioactive component of AM. Low binding energy between a ligand and the corresponding receptor indicates a stable conformation and a high possibility of action. The docking results showed that the binding energies of the 4 key targets were < -5 kJ·mol^{-1}, indicating that quercetin binds well to the key target protein (Table 5 and Fig. 13).

Table 5
Binding energies of quercetin for the key targets

bioactive component	key target	PDB ID	the binding energy(kJ·mol-1)
quercetin	*IL1β*	*5R8A*	-16.8615
quercetin	*CASP3*	*1QX3*	-6.73624
quercetin	*STAT1*	*6EEY*	-17.1544
quercetin	*PPARγ*	*7AWC*	-14.1419

4. Discussion

The results of our study showed that there are 24 compound targets of AM in LN. After PPI network analysis, we obtained 10 core targets according to degree value. Further, we performed ROC analysis to validate the core targets internally, and we found that the 10 core genes had high diagnostic values for LN, among which four key target genes, namely *CASP3*, *IL-1β*, *STAT1*, and *PPARγ*, had the highest diagnostic values. We also performed differential gene expression analysis on the external dataset

GSE99339, which showed that the 10 core genes had significant differential expression levels in LN. Further, molecular docking revealed that four key targets in LN had the highest binding properties to quercetin, the first bioactive component of AM. We performed GO and KEGG analyses on the 24 compound targets separately and found that the key target genes *CASP3* and *IL-1β* were enriched in the MAPK signaling pathway. Therefore, we speculated that AM suppresses LN by regulating inflammation at least through the MAPK signaling pathway.

Autophagy is an intracellular catabolic modality that maintains cellular homeostasis. Defects in autophagy are involved in the pathogenesis of SLE [7, 11, 12]. Studies have shown that autophagy is involved in the process of foot-cell injury in LN [13]. The MAPK cascade is a key signaling pathway regulating autophagy, cell proliferation and differentiation, apoptosis, and cellular stress response [14, 15]. This cascade inhibits autophagy by activating mTOR [16, 17]. Our findings revealed that the key target genes of AM in LN are enriched in the MAPK signaling pathway, and therefore we hypothesized that AM suppresses LN by regulating the MAPK signaling pathway. Indeed, autophagy is generally accompanied by apoptosis.

Caspase-3 is an essential member of the caspase family, an executor of the apoptotic pathway [18]. Several studies have shown activated caspase-3 in glomerular cells and infiltrated inflammatory cells (neutrophils and macrophages) in LN, and the increase in the number of apoptotic cells correlates with the severity of the glomerular lesions, demonstrating the involvement of apoptosis in the associated kidney injury [19]. Similarly, our analysis of the differentially expressed genes in LN revealed that caspase-3 expression increases in the kidneys of LN patients, and external datasets confirmed this result. We, therefore, hypothesize that regulation of caspase-3 expression may reduce apoptosis and thus treat LN.

In addition, our results showed increased expression of *IL-1β* in LN. Studies have demonstrated that the development of LN is closely related to inflammation [20]. *IL-1β* is involved in the pathogenesis of autoimmune diseases [21], and it acts as a pro-inflammatory cytokine and coordinates the inflammatory response by activating the NF-κB signaling pathway and promoting the release of cyclooxygenase-2 and interferon-γ [22]. In patients with LN, renal tubular epithelial cells play an essential role in the tubular interstitial inflammation by producing several inflammatory mediators, including interleukin (IL)-6 and *IL-1* [22–25]. Additionally, Castejon et al. have found that the active form of *IL-1β* directly contributes to the inflammatory damage in LN [26]. The p38MAPK signaling pathway promotes the development of LN by activating lymphocytes through the production and activation of inflammatory factors, such as monocyte chemotactic factor (*MCP-1*) and *IL-10*. A study by Liu et al. found that AM reduces the production of pro-inflammatory markers, such as *IL-1β*, and significantly inhibits the activation of *STAT1*, which in turn inactivates inflammatory cytokines [27]. Inflammation is closely related to autophagy; inflammatory mediators can inhibit autophagy, and impaired autophagy can also induce inflammatory responses. Therefore, we hypothesized that AM plays a role in regulating the expression of the key target gene *IL-1β*, which may be associated with the regulation of autophagy, to attenuate the inflammatory response and thereby improves the prognosis of LN.

Our study found that *PPARγ* and *STAT1* were also *significantly* upregulated and had diagnostic values for LN. Peroxisome proliferator-activated receptor γ (*PPARγ*), a nuclear transcription factor, can regulate thylakoid cell proliferation, prevent trans-differentiation, inhibit fibroblast proliferation and macrophage infiltration, and suppress inflammatory mediators. Activated *PPARγ* can ameliorate renal inflammation and fibrosis by inhibiting the TLR4/MyD88/NF-κB pathway [28]. Studies have shown that *STAT1* can accelerate the progression of LN by activating interferons, regulating the expansion and differentiation of T and B cells, and disrupting immune tolerance. Furthermore, the *STAT1* expression in peripheral blood mononuclear cells was elevated in patients with SLE, and this elevation correlates with disease activity [29]. *STAT1* has good binding properties for the first bioactive ingredient of AM. Therefore, we speculate that AM may also suppress LN by interfering with *PPARγ* and *STAT1*. However, the exact mechanism needs to be further explored.

In this study, we found that the key target genes of AM that are involved in the treatment of LN are all associated with quercetin, which is a vital bioactive component of AM and has anti-oxidative, anti-apoptotic, and anti-inflammatory properties [30, 31]. Quercetin can suppress hepatic fibrosis and atherosclerosis through signaling pathways, such as the MAPK and SIRT1 pathways, in hepatic and cardiovascular diseases [32, 33]. Studies have demonstrated that quercetin can play a therapeutic role in LN by inhibiting the activation of the nuclear factor-κB signaling pathway and suppressing the excessive proliferation of thylakoid cells. Accordingly, our results indicate that quercetin regulates the expression of caspase-3 and *IL-1β* through the MAPK signaling pathway, consequently regulating autophagy and suppressing apoptosis and cellular inflammatory response to treat LN.

This study has some limitations. First, the small sample size of the microarray data may have had some influence on the results. Second, although we performed clinical validation, the results of this study should be verified via extensive clinical studies and experimental validation.

5. Conclusion

In this study, we predicted that AM for LN might be related to inflammation and autophagy by combining network pharmacology, WGCNA, and molecular docking method, which provides a theoretical basis for clinical application of AM in the treatment of LN.

Abbreviations

AM	Astragalus membranaceus
AR	Androgen receptor
CASP3	Caspase-3
CCND1	Cyclin D1
CXCL10	C-X-C motif chemokine ligand 10
DL	Drug-likeness
EGF	Epidermal growth factor
ESRD	End-stage renal disease
GEO	Gene Expression Database
GO	Gene ontology
GS	Gene significance
IL-1β	Interleukin-1β
KDR	Kinase insert domain receptor
KEGG	Kyoto Encyclopedia of Genes and Genomes
LN	Lupus nephritis
MAPK	Mitogen-activated protein kinase
MCP-1	Monocyte chemotactic factor
ME	Module eigengene
MM	Modular membership
OB	Oral bioavailability
PDB	Protein Data Bank
PPARγ	Peroxisome proliferator-activated receptor γ
PPI	Protein-protein interaction
PTGS2	Prostaglandin-Endoperoxide Synthase 2
SLE	Systemic lupus erythematosus
STAT1	Signal transducer and activator of transcription 1
TCMSP	the Traditional Chinese Medicine Systems harmacology database
WGCNA	Weighted gene co-expression network analysis

Declarations

Acknowledgements

The research funding was supported by (International Cooperation of Shanxi Science and Technology) (Fund number: 201803D421063). The authors are very grateful for the data support provided by the European Renal Disease Database, TCMSP and GEO databases.

Authors contributions

Ting Liu, Xiaomei Qiao and Kaili Kong contributed equally to this work. Ting Liu, Xiaomei Qiao conceived and designed the study. Xiaomei Qiao and Kaili Kong wrote the manuscript. Kaili Kong coordinated and directed the project. Xiaoxia Wang, Rui Li and Ting Liu responsible for language modification. Xiaodong Zhang were responsible for revision of this manuscript for important intellectual content. All authors read and approved the manuscript.

Data availability

Data and materials from this study are available upon European Renal Disease Database, TCMSP and GEO databases.

Ethics declarations

The study data was based on public database, thus ethical approval is not required.

Competing interests

The authors declare no competing interests.

Footnotes

These authors contributed equally: Ting Liu, Xiaomei Qiao and Kaili Kong.

Supplementary information

Supplementary information is available.

ORCID IDs

Kaili Kong https://orcid.org/0000-0003-2475-7641

Xiaomei Qiao https://orcid.org/0000-0003-2224-827X

Xiaoxia Wang https://orcid.org/0000-0002-7473-6649

Rui Li https://orcid.org/0000-0001-9242-2929

Ting Liu https://orcid.org/0000-0001-6276-4063

Xiaodong Zhang https://orcid.org/0000-0003-3210-1407

References

1. Tsokos, G. C., Lo, M. S., Costa Reis, P. & Sullivan, K. E. New insights into the immunopathogenesis of systemic lupus erythematosus. *Nat Rev Rheumatol*, **12** (12), 716–730 https://doi.org/10.1038/nrrheum.2016.186 (2016).
2. Croca, S. C., Rodrigues, T. & Isenberg, D. A. Assessment of a lupus nephritis cohort over a 30-year period., **50** (8), 1424–1430 https://doi.org/10.1093/rheumatology/ker101 (2011).
3. Houssiau, F. A. & Ginzler, E. M. Current treatment of lupus nephritis. *Lupus*, **17** (5), 426–430 https://doi.org/10.1177/0961203308090029 (2008).
4. Shao, B. M. *et al.* A study on the immune receptors for polysaccharides from the roots of Astragalus membranaceus, a Chinese medicinal herb. *Biochem Biophys Res Commun*, **320** (4), 1103–1111 https://doi.org/10.1016/j.bbrc.2004.06.065 (2004).
5. Zhang, H. W., Lin, Z. X., Xu, C., Leung, C. & Chan L.S.. Astragalus (a traditional Chinese medicine) for treating chronic kidney disease. Cochrane Database Syst Rev 2014; (**10**); Cd008369. doi: 10.1002/14651858.CD008369.pub2.
6. Dos Santos, M. *et al.* Protective effects of quercetin treatment in a pristane-induced mouse model of lupus nephritis. *Autoimmunity*, **51** (2), 69–80 https://doi.org/10.1093/rheumatology/ker101 (2018).
7. Wu, D. J. & Adamopoulos, I. E. Autophagy and autoimmunity. *Clin Immunol*, **176**, 55–62 https://doi.org/10.1016/j.clim.2017.01.007 (2017).
8. Forli, S. *et al.* Computational protein-ligand docking and virtual drug screening with the AutoDock suite. *Nat Protoc*, **11** (5), 905–919 https://doi.org/10.1038/nprot.2016.051 (2016).
9. Wu, L. *et al.* Application of network pharmacology and molecular docking to elucidate the potential mechanism of Astragalus-Scorpion against prostate cancer. Andrologia 2021; **e14165**. doi: 10.1111/and.14165.
10. Xu, J. *et al.* Integration of network pharmacology and molecular docking technology reveals the mechanism of the herbal pairing of Codonopsis Pilosula (Franch.) Nannf and Astragalus Membranaceus (Fisch.) Bge on chronic heart failure. Ann Palliat Med. 2021; **10**(**7**); 7942-7959. doi: 10.21037/apm-21-1469.
11. Martinez, J. *et al.* Noncanonical autophagy inhibits the autoinflammatory, lupus-like response to dying cells. *Nature*, **533** (7601), 115–119 https://doi.org/10.1038/nature17950 (2016).
12. Rockel, J. S. & Kapoor, M. Autophagy: controlling cell fate in rheumatic diseases. *Nat Rev Rheumatol*, **12** (9), 517–531 https://doi.org/10.1038/nrrheum.2016.92 (2016).
13. Zhou, X. J., Klionsky, D. J. & Zhang, H. Podocytes and autophagy: a potential therapeutic target in lupus nephritis. *Autophagy*, **15** (5), 908–912 https://doi.org/10.1080/15548627.2019.1580512

(2019).

14. Castejon, M. L. *et al.* Dietary oleuropein and its new acyl-derivate attenuate murine lupus nephritis through HO-1/Nrf2 activation and suppressing JAK/STAT, NF-κB, MAPK and NLRP3 inflammasome signaling pathways. *J Nutr Biochem*, **74**, 108229 https://doi.org/10.1016/j.jnutbio.2019.108229 (2019).
15. Liu, F. C., Lee, H. C., Liao, C. C., Li, A. H. & Yu, H. P. Tropisetron Protects Against Acetaminophen-Induced Liver Injury via Suppressing Hepatic Oxidative Stress and Modulating the Activation of JNK/ERK MAPK Pathways. *Biomed Res Int*, **1952947**, https://doi.org/10.1155/2016/1952947 (2016).
16. Ba, L. *et al.* Allicin attenuates pathological cardiac hypertrophy by inhibiting autophagy via activation of PI3K/Akt/mTOR and MAPK/ERK/mTOR signaling pathways., **58**, 152765 https://doi.org/10.1016/j.phymed.2018.11.025 (2019).
17. He, Y. *et al.* p38 MAPK inhibits autophagy and promotes microglial inflammatory responses by phosphorylating ULK1. *J Cell Biol*, **217** (1), 315–328 (2018).
18. Mariño, G., Niso-Santano, M., Baehrecke, E. H. & Kroemer, G. Self-consumption: the interplay of autophagy and apoptosis. *Nat Rev Mol Cell Biol*, **15** (2), 81–94 https://doi.org/10.1038/nrm3735 (2014).
19. Du, X. S. *et al.* Wogonin attenuates liver fibrosis via regulating hepatic stellate cell activation and apoptosis. *Int Immunopharmacol*, **75**, 105671 https://doi.org/10.1016/j.intimp.2019.05.056 (2019).
20. Jeruc, J., Vizjak, A., Rozman, B. & Ferluga, D. Immunohistochemical expression of activated caspase-3 as a marker of apoptosis in glomeruli of human lupus nephritis. *Am J Kidney Dis*, **48** (3), 410–418 https://doi.org/10.1053/j.ajkd.2006.05.019 (2006).
21. Yung, S. & Chan, T. M. Molecular and Immunological Basis of Tubulo-Interstitial Injury in Lupus Nephritis: a Comprehensive Review. *Clin Rev Allergy Immunol*, **52** (2), 149–163 https://doi.org/10.1007/s12016-016-8533-z (2017).
22. Sims, J. E. & Smith, D. E. The IL-1 family: regulators of immunity. *Nat Rev Immunol*, **10** (2), 89–102 https://doi.org/10.1038/nri2691 (2010).
23. Conos, S. A., Lawlor, K. E., Vaux, D. L., Vince, J. E. & Lindqvist, L. M. Cell death is not essential for caspase-1-mediated interleukin-1β activation and secretion. *Cell Death Differ*, **23** (11), 1827–1838 https://doi.org/10.1038/cdd.2016.69 (2016).
24. Menke, J. *et al.* Colony-stimulating factor-1: a potential biomarker for lupus nephritis. *J Am Soc Nephrol*, **26** (2), 379–389 https://doi.org/10.1681/asn.2013121356 (2015).
25. Yung, S., Tsang, R. C., Sun, Y., Leung, J. K. & Chan, T. M. Effect of human anti-DNA antibodies on proximal renal tubular epithelial cell cytokine expression: implications on tubulointerstitial inflammation in lupus nephritis. *J Am Soc Nephrol*, **16** (11), 3281–3294 https://doi.org/10.1681/asn.2004110917 (2005).
26. Hao, W., Rovin, B. H. & Friedman, A. Mathematical model of renal interstitial fibrosis. *Proc Natl Acad Sci U S A*, **111** (39), 14193–14198 https://doi.org/10.1073/pnas.1413970111 (2014).

27. Wang, H. *et al.* Tubular basement membrane immune complex deposition is associated with activity and progression of lupus nephritis: a large multicenter Chinese study. *Lupus*, **27** (4), 545–555 https://doi.org/10.1177/0961203317732407 (2018).
28. Liu, C. M. *et al.* Quercetin protects mouse liver against nickel-induced DNA methylation and inflammation associated with the Nrf2/HO-1 and p38/STAT1/NF-κB pathway. *Food Chem Toxicol*, **82**, 19–26 https://doi.org/10.1016/j.fct.2015.05.001 (2015).
29. Michel, H. E. & Menze, E. T. Tetramethylpyrazine guards against cisplatin-induced nephrotoxicity in rats through inhibiting HMGB1/TLR4/NF-κB and activating Nrf2 and PPAR-γ signaling pathways. *Eur J Pharmacol*, **857**, 172422 https://doi.org/10.1016/j.ejphar.2019.172422 (2019).
30. He, Y. *et al.* Quercetin induces autophagy via FOXO1-dependent pathways and autophagy suppression enhances quercetin-induced apoptosis in PASMCs in hypoxia. *Free Radic Biol Med*, **103**, 165–176 https://doi.org/10.1016/j.freeradbiomed.2016.12.016 (2017).
31. Iris, M., Tsou, P. S. & Sawalha, A. H. Caffeine inhibits STAT1 signaling and downregulates inflammatory pathways involved in autoimmunity. *Clin Immunol*, **192**, 68–77 https://doi.org/10.1016/j.clim.2018.04.008 (2018).
32. Basu, A., Das, A. S., Majumder, M. & Mukhopadhyay, R. Antiatherogenic Roles of Dietary Flavonoids Chrysin, Quercetin, and Luteolin. *J Cardiovasc Pharmacol*, **68** (1), 89–96 https://doi.org/10.1097/fjc.0000000000000380 (2016).
33. Wang, R., Zhang, H., Wang, Y., Song, F. & Yuan, Y. Inhibitory effects of quercetin on the progression of liver fibrosis through the regulation of NF-κB/IκBα, p38 MAPK, and Bcl-2/Bax signaling. *Int Immunopharmacol*, **47**, 126–133 https://doi.org/10.1016/j.intimp.2017.03.029 (2017).

Figures

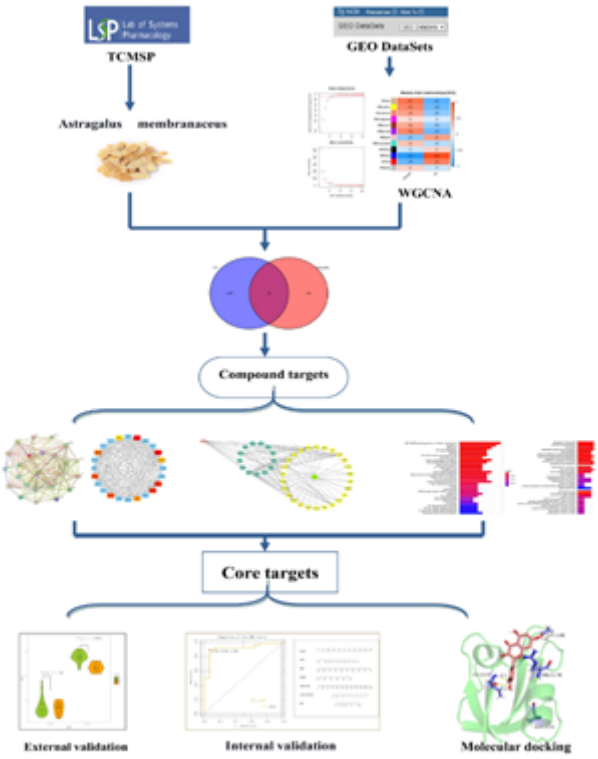

Figure 1

The flow diagram of the study.

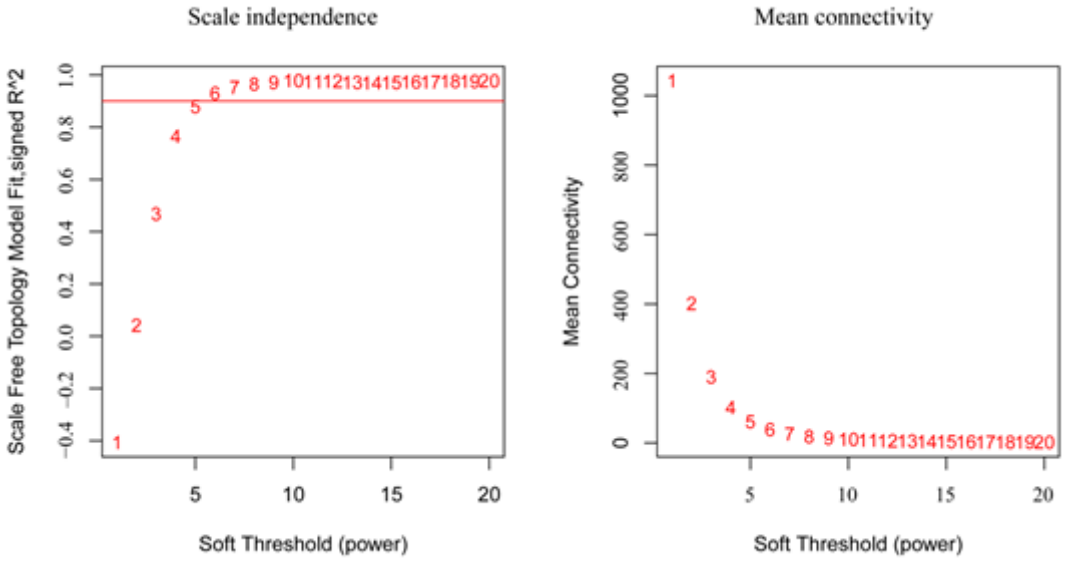

Figure 2

Analysis of soft-thresholding values from 1 to 20.

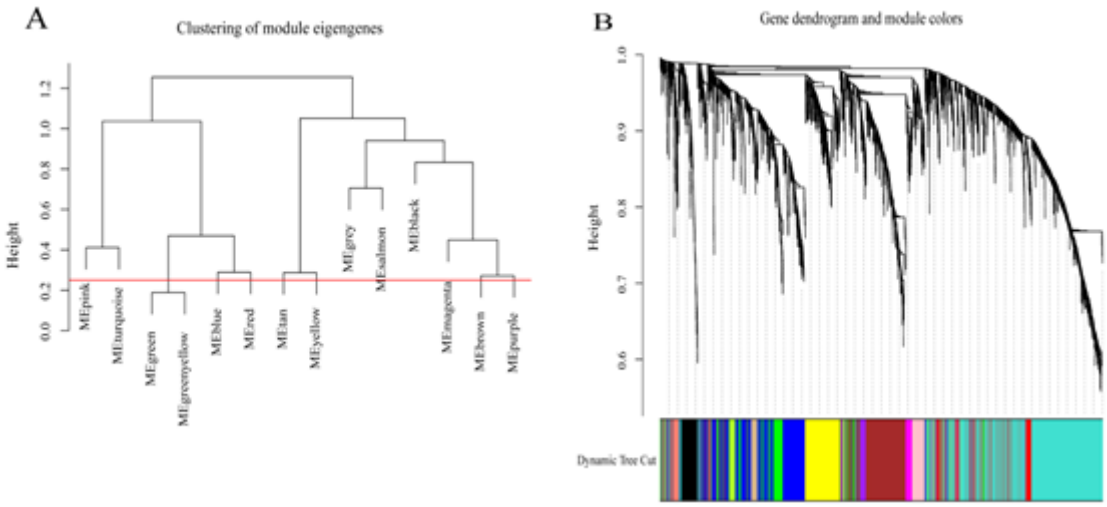

Figure 3

(A) Cluster dendrogram of dataset genes after dynamic cutting. Clustering of module eigengenes by setting "minimum module size = 50 and cut height = 0.25". (B) Module-trait relationships Genes within different modules are labeled with different colors according to WGCNA's conventions.

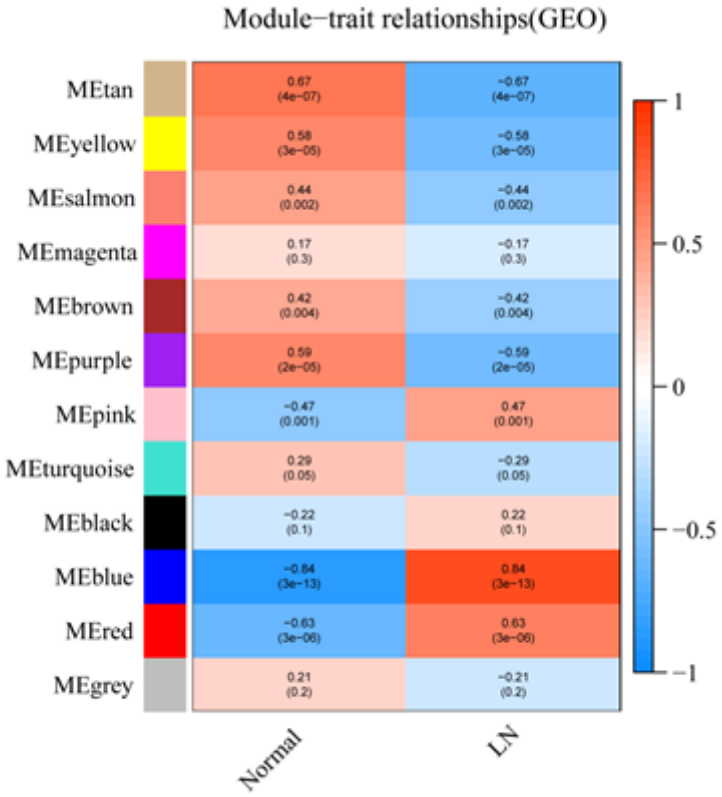

Figure 4

Heatmap of correlations between module genes and clinical traits.

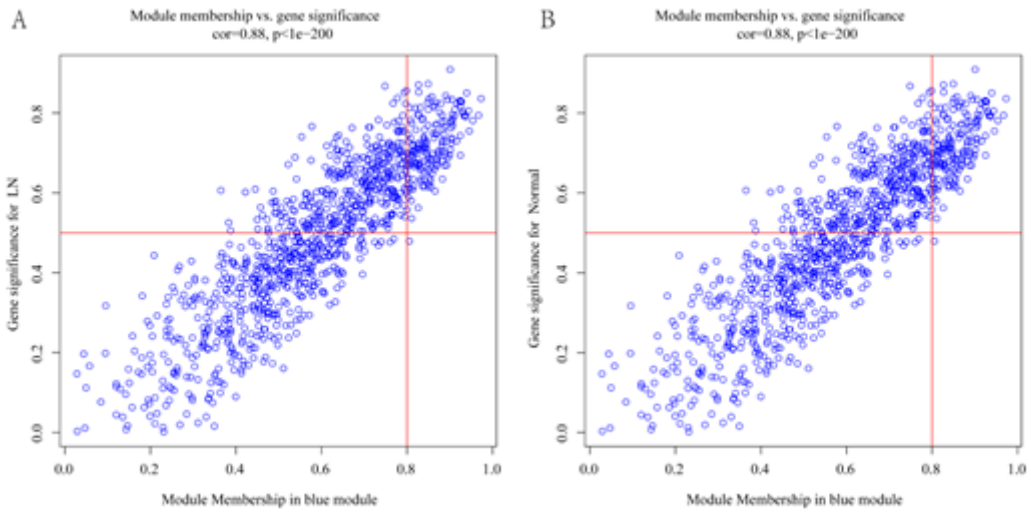

Figure 5

The connectivity alongside the importance of the genes within the blue modules in the LN(A) and healthy groups (B), $p < 0.05$.

Figure 6

The Venn diagram of genes among of AM-LN-related targets.

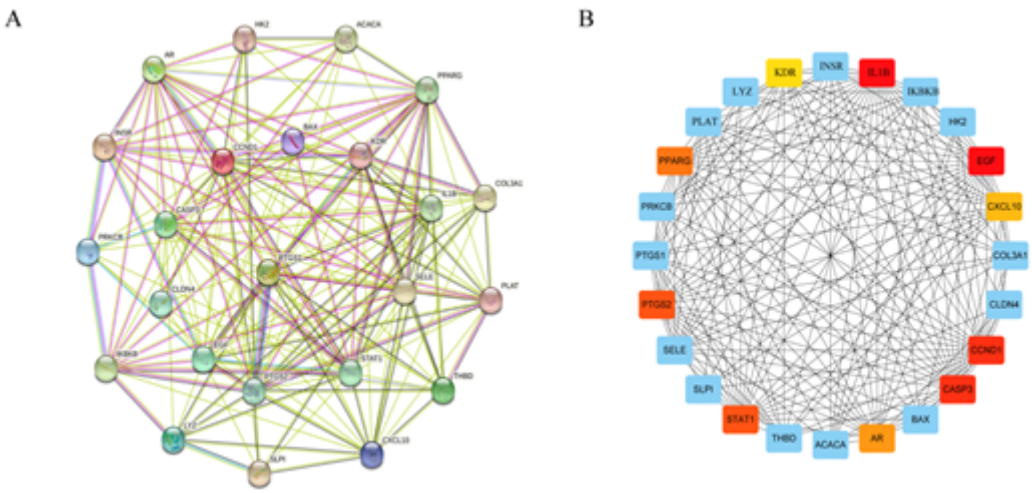

Figure 7

Visualization of the protein-protein interaction (PPI) network and the candidate hub genes. (A) PPI network of the compound targets. (B) Identification of the core genes from the PPI. The red nodes represent genes with a high degree value,while the yellow node represent genes with a low degree value.

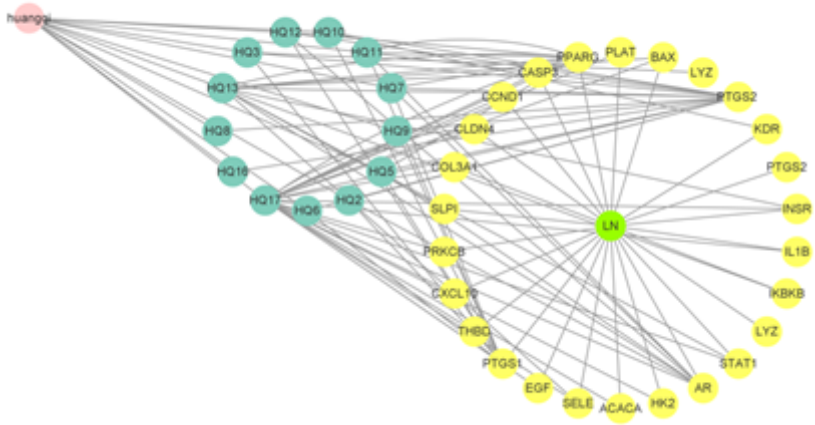

Figure 8

"Drug-bioactive ingredients-compound targets-disease" interaction network.

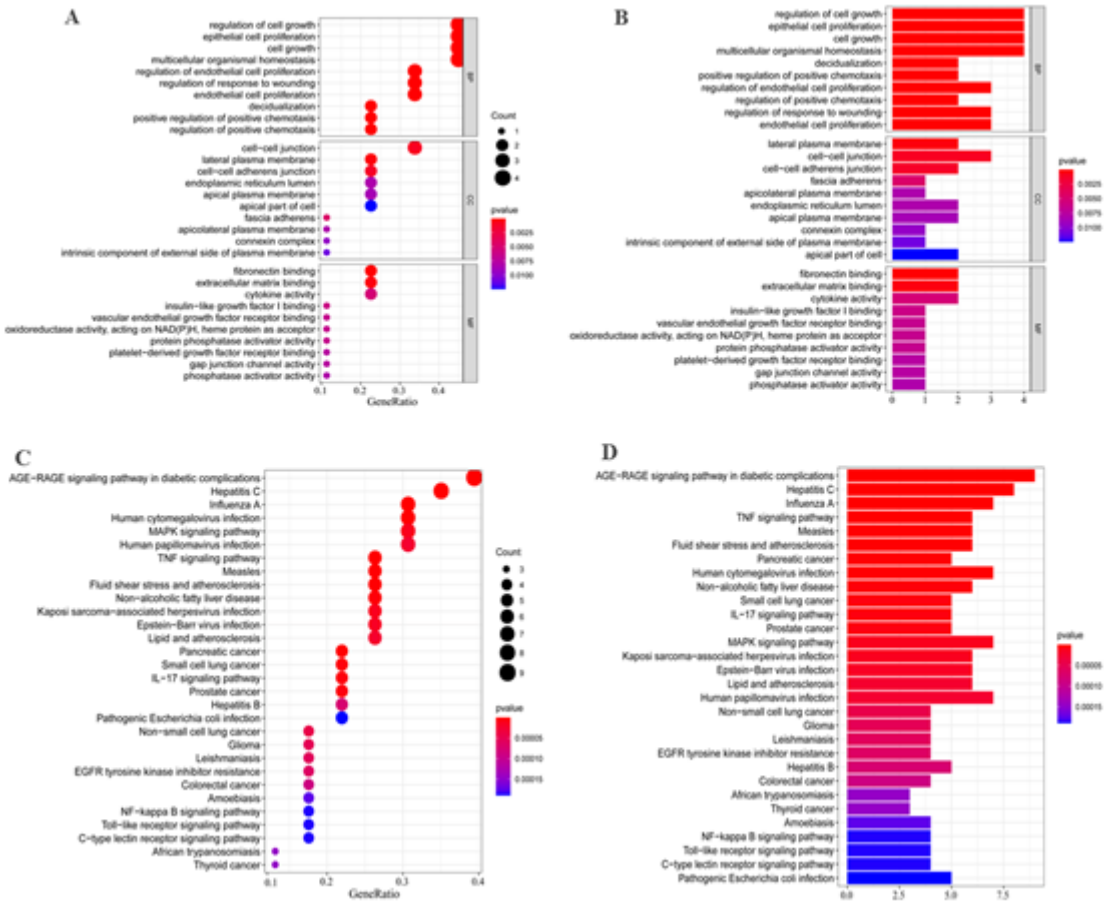

Figure 9

GO and KEGG enrichment analyses of compound targets. (A) results of GO enrichment analyses; (B) results of KEGG enrichment analyses.

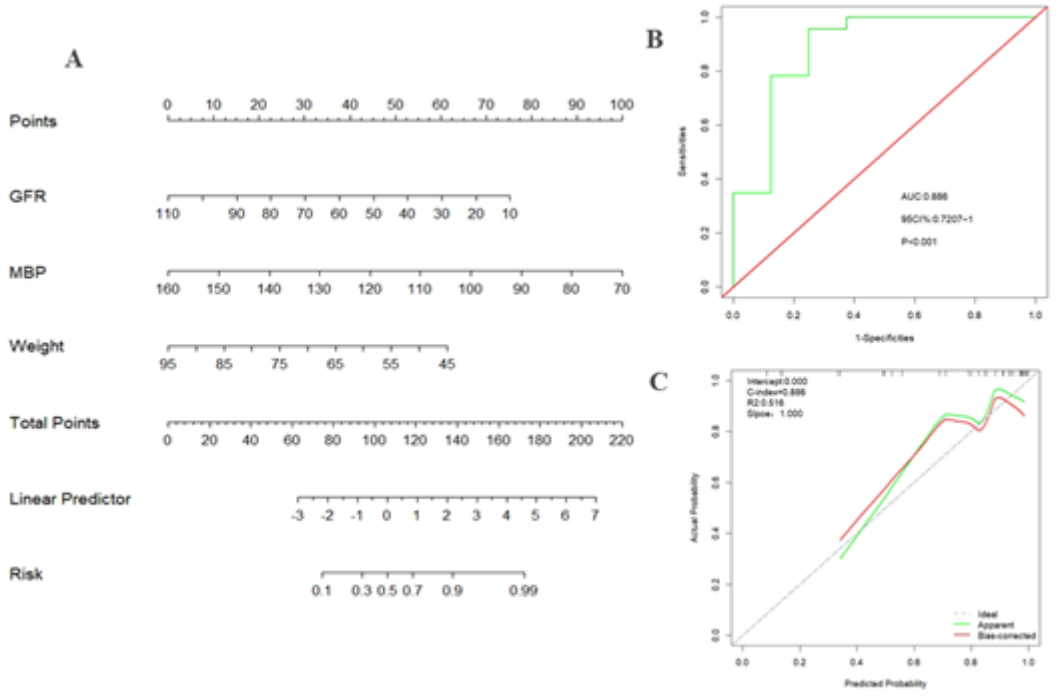

Figure 10

Nomogram and it's validation. (A) Nomogram for predicting the risk of LN. (B) ROC Curve for predicting LN risk with Column Line Graph Model. (C) The calibration curve predicting the risk of LN by the nomogram and the actual risk.

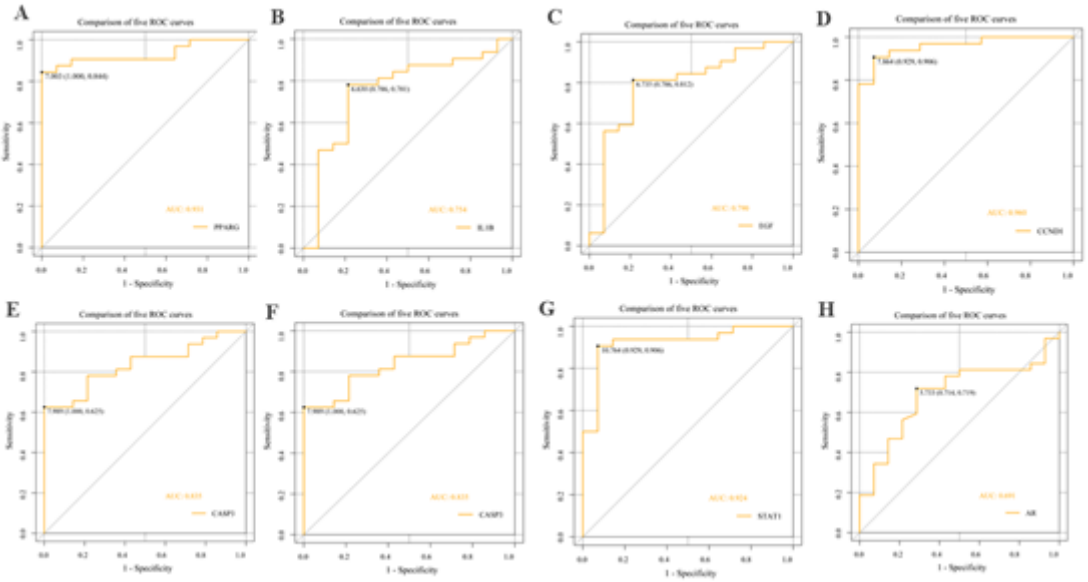

Figure 11

ROC analysis of 10 core genes in GSE32591 dataset. (A) ROC analysis of PPARγ in GSE32591 dataset. (B) ROC analysis of IL1β in GSE32591 dataset. (C) ROC analysis of EGF in GSE32591 dataset. (D) ROC analysis of CCND1 in GSE32591 dataset. (E) ROC analysis of CASP3 in GSE32591 dataset. (F) ROC analysis of STAT1 in GSE32591 dataset. (G) ROC analysis of PTGS2 in GSE32591 dataset. (H) ROC analysis of AR in GSE32591 dataset. The larger the AUC value, the higher the diagnostic value for LN.

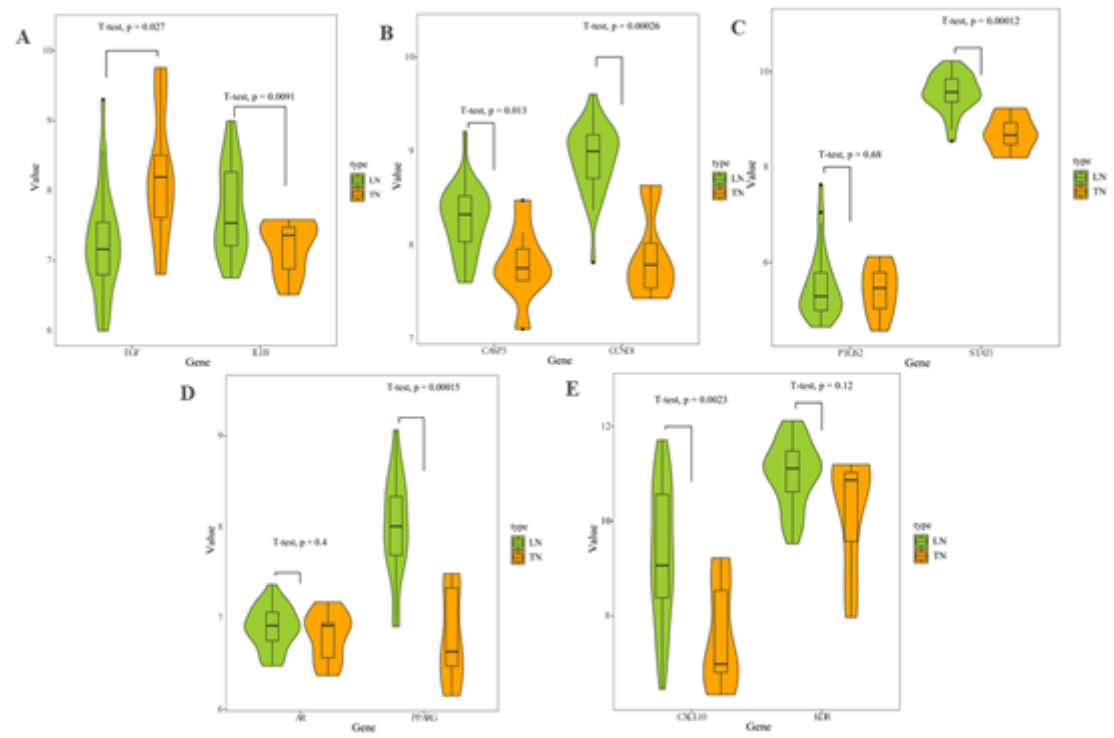

Figure 12

Validation of expression levels of the ten core genes in GSE99339 dataset. (A) Gene expression value EGF and IL1β among samples of GSE99339 dataset. (B) Gene expression value CASP3 and CCND1 among samples of GSE99339 dataset. (C) Gene expression value STAT1 and PTGS2 among samples of GSE99339 dataset. (D) Gene expression value PPARγ and AR among samples of GSE99339 dataset. (E) Gene expression value CXCL10 and KDR among samples of GSE99339 dataset.

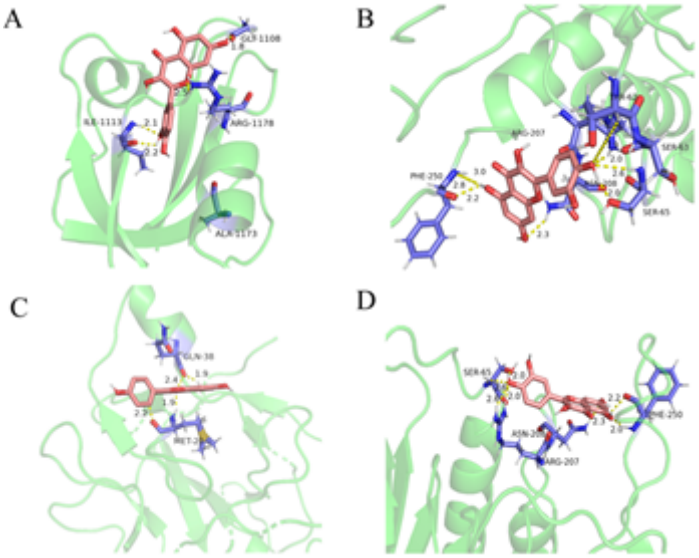

Figure 13

The detailed target-compound interactions of the docking simulation. (A) Molecular docking of quercetin binding site of STAT1. (B) Molecular docking of quercetin binding site of PPARγ. (C) Molecular docking of

quercetin binding site of IL-1β. (D) Molecular docking of quercetin binding site of and CASP3.